A CONSTRAINT SATISFACTION PROBLEM APPROACH TO HIGH-ENTROPY ALLOY DESIGN

An Undergraduate Research Scholars Thesis

by

ANAS ABU-ODEH

Submitted to the Undergraduate Research Scholars program at
Texas A&M University
in partial fulfillment of the requirements for the designation as an

UNDERGRADUATE RESEARCH SCHOLAR

Approved by Research Advisor: Dr. Raymundo Arroyave

May 2017

Major: Mechanical Engineering

TABLE OF CONTENTS

ABSTRACT

A Constraint Satisfaction Problem Approach to High-Entropy Alloy Design

Anas Abu-Odeh
Department of Mechanical Engineering
Texas A&M University

Research Advisor: Dr. Raymundo Arroyave
Department of Materials Science and Engineering
Texas A&M University

High-entropy alloys (HEAs) are multi-principal element alloys at near-equiatomic concentrations that can have superior properties such as high irradiation resistance, high fatigue resistance, and high temperature usage, compared to conventional alloys. Because of their properties, HEAs may find applications in industries such as nuclear, aerospace, medical, and electronic. However, the design and discovery of HEAs has been largely limited to trial and error, Edisonian, methods, and only a fraction of the possibilities have been produced. A computational alloy design methodology using the constraint satisfaction problem (CSP) approach is proposed to accelerate the design and discovery of HEAs. This approach consists of three major steps: mapping design requirements into mathematical constraints and using computational thermodynamic calculations to implement them, sampling the HEA space of composition and temperature within the constraints to search for solutions, and describing the final solution space using machine learning methods. Ultimately, the CSP approach enables the identification of potentially all regions in composition space that satisfy material design requirements. A Thermo-Calc database used to encode the thermodynamic information of all phases in a given alloy system was verified against experimental data to be implemented for

phase stability calculations. With kinetic considerations, 70.8% of the 216 evaluated alloys showed good agreement between experiments and calculations using the database. This database was used to map out single-phase solid solution regions for the known CoCrFeMnNi HEA and all its subsequent near-equiatomic quaternary and ternary systems. Afterwards, regions of possible precipitation hardening potential were determined in the AlCoCrFeNi system. The results demonstrate the CSP algorithm's capability to search HEA thermodynamic space and to accelerate HEA design and discovery.

ACKNOWLEDGEMENTS

I would like to thank Dr. Raymundo Arroyave for his guidance in this research, as well as Nayan Chaudhary, for helping me during the database verification process, and Sean Gibbons, whose use of the CSP approach in a previous project allowed me to understand how to interface between Thermo-Calc and MATLAB.

I would also like to thank Dr. Richard Malak's group for their help with the CCSA. Edgar Galvan created and provided the algorithm, and he, along with Tanner Kirk, helped with debugging the algorithm and conceptual clarity.

I would also like to thank Thermo-Calc Software for their interest in this project, their provision of the TCHEA1 database, and the creation of Figures A1 and A2. The people involved include Huahai Mao, Qing Chen, and Paul Mason.

I would also like to thank Jules Henry, who brought the Undergraduate Research Scholars program to my attention and suggested that I join.

CHAPTER I

INTRODUCTION

High-entropy alloys (HEAs) have received much attention in recent years because they have expanded the alloy design space and led to the discovery of alloys with unique and high-performance properties. HEAs are alloys with five or more components at near-equiatomic concentrations (generally 5-35%) [1]. They can have properties such as high irradiation resistance, high operating temperatures, or constant electrical resistance values at varying temperatures making them deployable as structural or functional materials in a wide range of industrial applications [2,3]. Traditional alloy design has largely been limited to the "edges" and "corners" of composition space, where alloys are made with one or two dominant elements [4]. The space in between these "edges" and "corners" are where components start to have near-equal concentrations in alloy composition. Given all the possible alloying elements, and other variables such as temperature and pressure, this search space has many dimensions. There is plenty to explore, and methodologies to help accelerate this process are in need. Exhaustive experimental or computational approaches to find new HEA compositions are costly in time and resources. An efficient way to search through HEA space is needed to circumvent this limitation.

Materials research typically follows the trend of looking at a material composition, evaluating its structure at certain conditions, determining the properties of the material, and testing its performance. Exhaustive methods, such as high-throughput or grid searches, involve iterating over this process many times. Materials design deals with the inverse approach, which involves defining the desired criteria that a material performs against, finding the properties

required to match this performance, and determining the composition and structure that a material would need to have these properties. Instead of exploring with an exhaustive approach, a computational constraint satisfaction problem (CSP) approach would be fitting for exploring the HEA space [5]. This involves defining constraints, sampling a search space, and evaluating samples against the constraints. The goal is to find the sample region that fits within the boundary of the solution space that satisfies the constraints. In HEA exploration, the constraints could be a minimum or maximum phase fraction of solid solution, or the ability to precipitate harden.

In this study, the HEA composition of CoCrFeMnNi, a commonly cited HEA [6], is evaluated through the CSP approach. The CSP approach is embodied through a continuous constraint satisfaction algorithm (CCSA) that uses a genetic algorithm to sample composition and temperature space for points to compare against the constraints [5]. These points are evaluated using Thermo-Calc software, which uses the minimization of the Gibbs free energy of the system, given values of temperature, pressure, and composition, to predict the most stable phase composition. Thermo-Calc's TCHEA1 database, an HEA thermodynamic database that uses fifteen different elements, and the CCSA are coupled to find the single-phase solid solution regions in all the possible ternary, quaternary, and quinary combinations of CoCrFeMnNi. Before doing so, the TCHEA1 database was verified against experimental literature [7]. This was done by looking at 216 HEA compositions whose phases were experimentally determined and comparing those observations to calculations in Thermo-Calc. This database was used in conjunction with the CCSA to evaluate near-equatiomic concentrations of CoCrFeMnNi and its ternary and quaternary compositions. These results show that the CCSA can be used to explore

materials design spaces of three, four, and five dimensions (including temperature) to determine whether a composition is a single-phase solid solution. Afterwards, the $Al_xCoCrFeNi$ composition was evaluated with the TCHEA1-CCSA framework to find solution spaces that can be precipitate hardened. The use of this framework provides a way to accelerate HEA design and discovery by providing a vessel to explore between the “edges” and “corners” of alloy design space.

CHAPTER II

METHODS

Verification of TCHEA1

Thermo-Calc's TCHEA1 thermodynamic database for HEAs uses fifteen elements: Al, Co, Cr, Cu, Fe, Hf, Mn, Mo, Nb, Ni, Ta, Ti, V, W, and Zr. It was verified against experimental data before its use with the CCSA. The verification involved searching through experimental HEA literature, calculating the phase stability of observed HEAs using TCHEA1, and comparing experimental phase observations against calculations. The experimental compositions act as inputs into Thermo-Calc, which outputs phase stability graphs (such as Figure A1 in Section A of the Appendix). The graphs show different phases fractions at different temperatures. The experimental phase observations were collected from articles cited in a compiled table [7]. From this table, 216 HEAs that could be described by the database were identified as candidates for verification.

Thermo-Calc's TCHEA1 database has both disordered and ordered phases listed. However, the designation for a disordered phase, such as BCC_A2 or FCC_A1, does not appear when the phase is disordered. Instead, the ordered phase designations, BCC_B2 or FCC_L12, appear for the BCC or FCC phases regardless of the ordering. Therefore, site fraction calculations are required to classify the phases as ordered or disordered. For example, the ordered BCC_B2 structure contains two sublattices. If this phase is ordered, then the site fraction of an element in one sublattice will be different than the site fraction of the same element in another sublattice. This is due to the partitioning and ordering of elements between the

sublattices. If the phase is disordered, then an element will have an equal chance of being in either of the two sublattices. Thus, the site fractions of an element will be the same.

Phase observations and alloy compositions from experimental papers [1, 6, 8-58] were recorded in an Excel sheet. If a certain article was not found from the compiled table, the phases mentioned in the compiled table were used for comparison.

CCSA methodology

The CCSA is comprised of multiple stages: the definition of constraints, the sampling of the search space, the evaluation of the samples against the constraints, and the description of the solution space. The definition of constraints creates a boundary for the solution space to fill. The goal of this approach is to find the boundary that encompasses all the points that can satisfy the constraints. These constraints are user-defined inputs that represent the desired properties to be found in the search space.

Before sampling the search space, its dimensions must be defined. Since the constraints in this study deal with phase stability calculations, the inputs that Thermo-Calc requires are composition, temperature, and pressure. Pressure is assumed to be 100000 Pa, approximately atmospheric pressure, for all cases. The temperature and composition ranges are described later for different scenarios.

Different approaches, such as a genetic algorithm or a bi-section method, have been employed as part of a CCSA to find feasible solution spaces [5, 59]. This study was done using a

genetic algorithm approach. Firstly, an initial population set which satisfies the constraints must be defined. In this study, the initial population is found by a search evaluating random points against the constraints. Once a determined number of points that satisfy the constraints are found (representing the first generation), the genetic algorithm creates a new generation biased towards the desirable constraints. Genetic algorithms are traditionally used for minimum/maximum optimization, which generally means converging to a point. However, this study requires the algorithm to converge towards a boundary that satisfies the constraints. This means that the next generation will be created from parents that are at the furthest from the center of the previous generation. This iteration will continue until a specified number of generations have been created.

Since the constraints in this study deal with phase stability, the constraint evaluation will consist of phase stability calculations in Thermo-Calc. The inputs of composition, temperature, and pressure will be used to find the phase stability through the minimization of the Gibb's free energy equation, using parameters from the TCHEA1 database.

The solution space is described by the boundaries that encompass it. The CCSA can generate a computationally inexpensive approximation of the boundary. This has a lower cost than a brute-force approach such as a grid-search. Experimental and computational researchers can avoid searching through step-iteration, and can instead guide their studies with a presented solution space.

If an initial generation is created, the CCSA will continue to create generations with a user-specified population size until it creates the user-specified amount of generations. If no initial generation is created, the CCSA will keep searching. To avoid a long search time, this study includes a termination criterion when no initial generation is created after the number of point evaluations exceeds that of the number of required generations squared, causing the CCSA to end. This is considered as a scenario that does not pass the constraints.

Defining and implementing the constraints

Below are the descriptions of the constraints that are input into the CCSA to describe a system that is a single-phase solid solution or to determine whether a system can be precipitate hardened.

Single-phase solid solution search

In all the different near-equiatomic compositions, the temperature range was between 500 K and 2000 K. Composition is given as a range of about +/- 5% from the pure equiatomic concentration. This is done because the definition of an HEA is given as "near-equiatomic," which implies discretion on the user to what "near" means. The solid solution region is that where at least 99% of the phase present is either a BCC, B2, FCC, L12, or HCP phase. As stated before, the TCHEA1 database does not distinguish between the BCC and B2 phase, or the FCC and L12 phase. To distinguish between the BCC and B2 or FCC and L12 phases from the TCHEA1 database, site fraction data was evaluated from Thermo-Calc. If the site fractions of any element in the two different sublattices were different, then it was an ordered phase (B2 or L12). Otherwise, it was a disordered phase (BCC or FCC).

The CoCrFeMnNi system has ten possible ternaries that can form from the five different elements: CoCrFe, CoCrMn, CoCrNi, CoFeMn, CoFeNi, CoMnNi, CrFeMn, CrFeNi, CrMnNi, and FeMnNi. An equitomic concentration would result in each element contributing to about 33% of the composition. This makes the domain of the composition search space for each element to be 28-38%. This is a three-dimensional problem, with two of the dimensions being two of the compositions in the ternary (the third composition is the difference between 100% and the sum of the other two compositions) and the last dimension is temperature. The amount of generations created during the genetic algorithm is 75, with each generation having a population of 75 points.

The CoCrFeMnNi system has five possible quaternaries that can form from the five different elements: CoCrFeMn, CoCrFeNi, CoCrMnNi, CoFeMnNi, and CrFeMnNi. A purely equiatomic concentration would result in each element contributing to 25% of the composition. The domain of the composition search space for each element is 20%-30%. This is a four-dimensional problem, with three of the dimensions being compositions and the last being temperature. The amount of generations created is 150, with each generation having a population of 150 points.

The CoCrFeMnNi system has an equiatomic composition when each of its elements is at 20%. The domain of the composition space search for here is from 15-25%. This is a five dimensional problem with four of the dimensions being four of the compositions and the last dimension being temperature. The amount of generations created is 200, with each generation having a population of 200 points.

Determining precipitate hardenability

The AlCoCrFeNi system was observed to have B2 precipitates in an FCC matrix at a certain composition [60]. Using the CCSA, the temperature and composition space where this system can be precipitate hardened was searched. The composition space looked at was 10-30% of each of the elements. The next constraint was to search between 1500 K and 1800 K for a single-phase solid solution region. If a solid solution region is found, the algorithm subtracts 100 K from the current temperature to find a two-phase region. Figure A2 in Section A of the Appendix shows an isopleth that has a two-phase region in a lower temperature than a single-phase solid solution region. The algorithm will continue subtract 100 K until it finds a two-phase region. If this is not found before 500 K, the algorithm considers this a failed search (the kinetics for nucleation are assumed to be extremely slow to be significant at this point). If a two-phase region is found, the phases are compared against the following criteria. First, the two phases must not result from spinodal decomposition. This means that if the primary phase is a BCC, B2, FCC, L12, then the second phase cannot be the same respective phase with a different chemical composition. Second, if the primary phase is an ordered phase (B2, L12), then the secondary phase cannot be its disordered counterpart (BCC, FCC, respectively). If a composition passes these criteria, it is determined to have the potential to precipitate harden. The amount of generations created is 200, with each generation having a population of 200 points.

CHAPTER III

RESULTS

TCHEA1's agreement with experimental data

When looking at the compiled table of experimental data from Ref. 7, some of the phase observations did not match the articles that were referenced in the table. It was necessary to look at the as many of the cited articles, which describe the 216 alloys being looked at, as possible to verify that the phases reported in the table were correct. For example, the alloy $AlCrCuFeNi_2$ was reported to show only an FCC phase in the table [7], but the actual experiments report FCC+BCC phases [46]. Matches were classified based on what phases the articles reported, and if those phases are present when the experimental composition and temperature is input into Thermo-Calc using the TCHEA1 database.

An important kinetic consideration is the as-cast state of the alloys in most of the experiments. When an alloy is processed through traditional casting, the heat from the liquid phase dissipates to the surroundings quickly, since there is a large thermal gradient. This rapid cooling may not allow for certain phases, which may be described in Thermo-Calc phase fraction graphs, to have enough time to precipitate. Thermo-Calc is a thermodynamic software, so kinetics are not taken into account. Due to this, the phases shown in Thermo-Calc which do not appear in experimental data could be different phases initially, but if the sample has infinite time for diffusion (the assumption made in Thermo-Calc), the phase may theoretically appear.

70.8% of the 216 alloys matched with kinetic considerations across experimental data and calculations from the TCHEA1 database. To explain the mismatches, a deeper understanding of crystallography, thermodynamics, kinetics, and experimental techniques is needed. However, the database's 70.8% match is adequate for implementing it with the CCSA.

Single-phase solid solution regions

Below are the results and some plots of the search for single-phase solid solution regions in the ternaries, quaternaries, and quinary of CoCrFeMnNi. The results also include precision, recall, and misclassification metrics for one ternary, one quaternary, and the quinary. These metrics serve as an example of how reliable the CCSA can be. Precision represents the fraction of data in the boundary solution output by the CCSA that belongs to the target data (in this case, the classification is single-phase solid solution). Recall is the fraction of target data that falls in the boundary solution. The misclassification rate is the fraction of data that is placed in the wrong classification. The method of calculating these metrics was adapted from Galvan [59] using 10^6 random phase stability data points generated from Thermo-Calc. These data points were within the temperature and composition ranges of the respective alloy.

Ternaries

Table 1 shows the calculated solid solution single-phases in the ternaries, except for CrMnNi (denoted by an asterisk in Table 1), which failed the CCSA through the termination criteria. However, there is a temperature range in which the equiatomic ternary of CrMnNi has around 80% of the L12 phase (the blue line in Figure A3 in Section A of the Appendix). This was verified to be an ordered phase through site fraction comparisons.

Table 1. Single-phase solid solutions in ternary alloys

Ternary Composition	Ternary Solid-Solution Phase	Temperature Range (K)
CoCrFe	BCC, FCC	1572 – 1695, 1178 – 1681
CoCrMn	BCC, HCP	1107 – 1540, 645 – 1034
CoCrNi	FCC	819 – 1716
CoFeMn	FCC	745 – 1581
CoFeNi	FCC	880 – 1731
CoMnNi	L12	688 – 1487
CrFeMn	BCC	1324 – 1713
CrFeNi	FCC	1044 – 1672
FeMnNi	L12	542 – 1509
CrMnNi*	L12	None

The CCSA algorithm outputs the boundary regions for spaces where the alloys pass the constraints. These boundaries can be visualized with plots like the one shown in Figure 1, where the regions of single-phase BCC (blue) and HCP (green) in CoCrMn that can be formed in the given temperature and composition range can be seen. The visualization of the other ternaries can be seen in Section B of the Appendix.

The CCSA also quantifies the boundary numerically. This can be used to determine whether a specific data point lies within the constraints. Using this method to classify 10^6 random points in the CoCrMn temperature and composition space allows for the determination of the precision, recall, and misclassification rate of the boundary classification. These values were found to be 94.68%, 90.87%, and 1.94%, respectively.

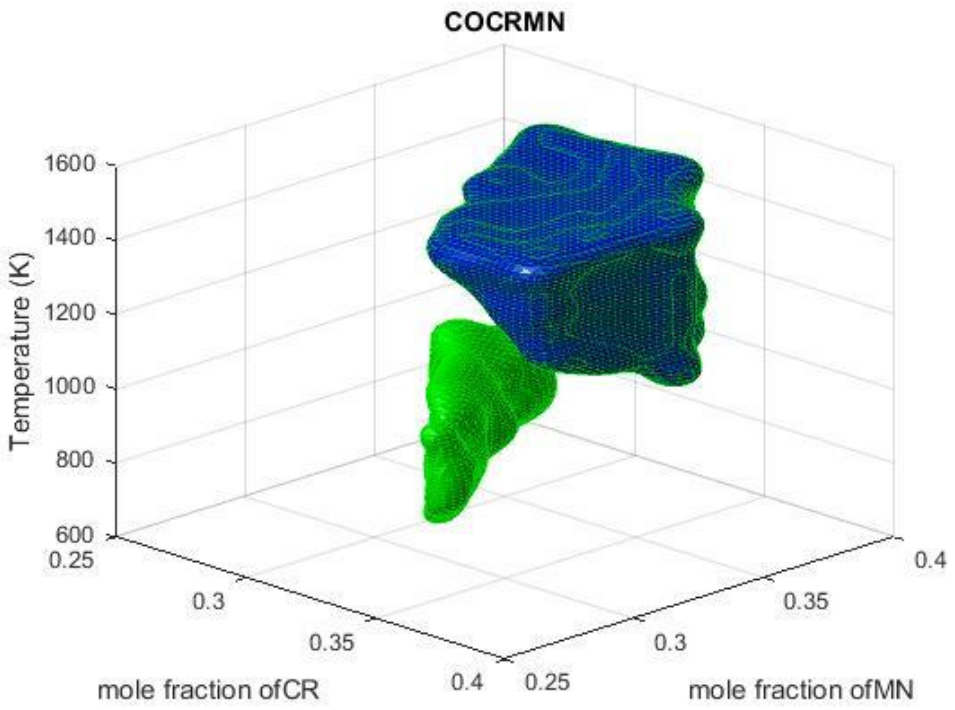

Figure 1. Single-phase regions for BCC and HCP in CoCrMn

Quaternaries

Table 2 shows the calculated solid solution single-phases in the quaternaries. The FCC single-phase region in CoCrMnNi (denoted by an asterisk) is significantly small compared to the L12 region.

Table 2. Single-phase solid solutions in quaternary alloys

Quaternary Composition	Quaternary Solid-Solution Phase	Temperature Range (K)
CoCrFeMn	BCC, FCC	1325 – 1606, 986 – 1585
CoCrFeNi	FCC	827 – 1726
CoCrMnNi	FCC*, L12	1448 – 1474, 677 – 1548
CoFeMnNi	L12	766 – 1573
CrFeMnNi	L12	1009 – 1548

The boundaries of these regions can also be visualized, like that of the ternaries. However, the quaternary searches have an extra dimension than the ternary searches because of the extra component. Therefore, the quaternary regions of single-phase solid solutions are represented in multiple plots, with the temperature dimension being "frozen" at a value. This is shown in the plots of CoCrFeMn (Figure 2), where the regions of FCC (red) feasibility decrease while regions of BCC (blue) feasibility increase with an increase in temperature. The other quaternary visualizations are in Section C of the Appendix. The precision, recall, and misclassification rates for the classification of the phases of CoCrFeMn are 93.5%, 72.39%, and 1.03%, respectively.

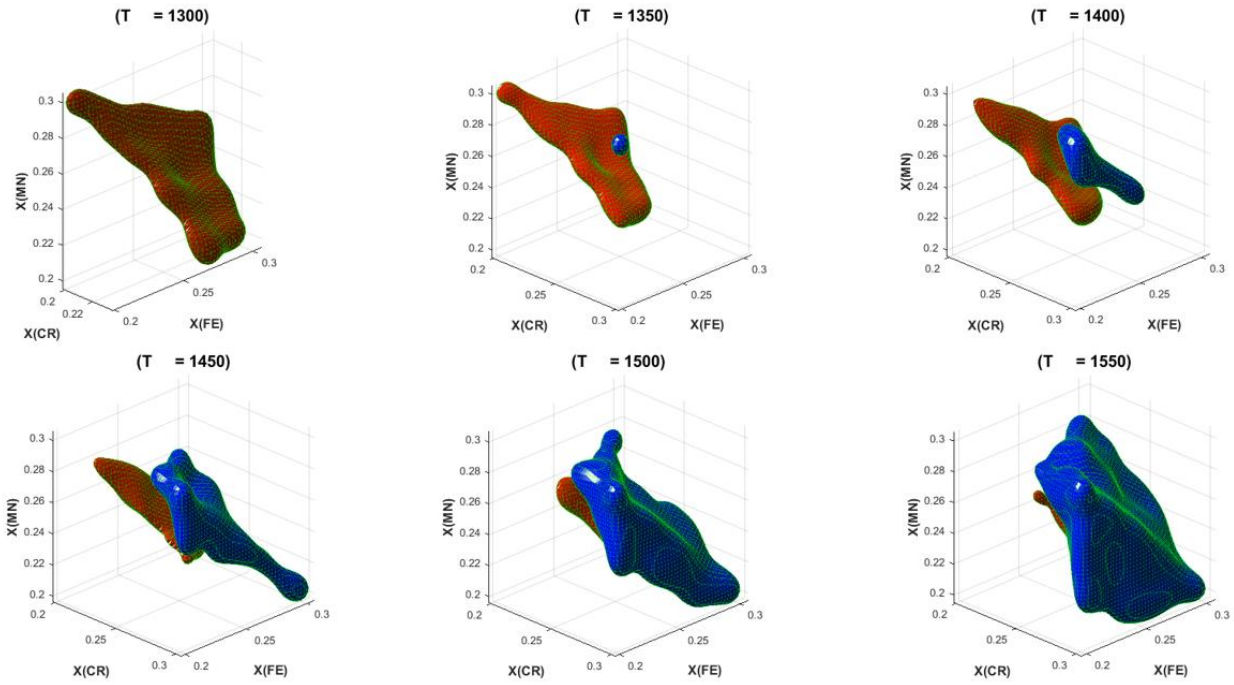

Figure 2. Evolution of CoCrFeMn's single-phase solid solution regions over varying temperature

Quinary

The main single-phase solid solution region found in the CoCrFeMnNi alloy is that of the ordered L12 phase in the temperature range of 751 – 1601 K. The CCSA boundary solution only shows a small region of a disordered FCC phase in the temperature range of 1280 – 1558 K. This is surprising because the CoCrFeMnNi alloy is one that is commonly cited as having a disordered FCC phase [6]. The L12 phase is an ordered version of the FCC phase. Since Thermo-Calc's TCHEA1 database will label both an FCC and L12 phase as FCC_L12, the site fractions must be observed to determine whether it is an FCC or L12 phase. Figure A4 shows the site fractions of the FCC_L12 sublattices for the equiatomic CoCrFeMnNi composition. Lines 1-5 represent the site fractions for elements in the first sublattice, and lines 6-10 represent the site fractions for the second sublattice. Since the lines are not on top of each other, this represents an ordered phase. However, the difference in the site fractions are small, around 0.02, which could mean that the difference in element partitioning is not significant. This could be due to an error in Thermo-Calc's calculation.

The visualization for the change in the L12 (magenta) region with respect to temperature and concentration of Ni in the CoCrFeMnNi alloy can be seen in Figure 3. The FCC region is not shown because it is too small a region to visualize. The precision, recall, and misclassification rate for this classification are 83.64%, 97.69%, and 5.02%, respectively.

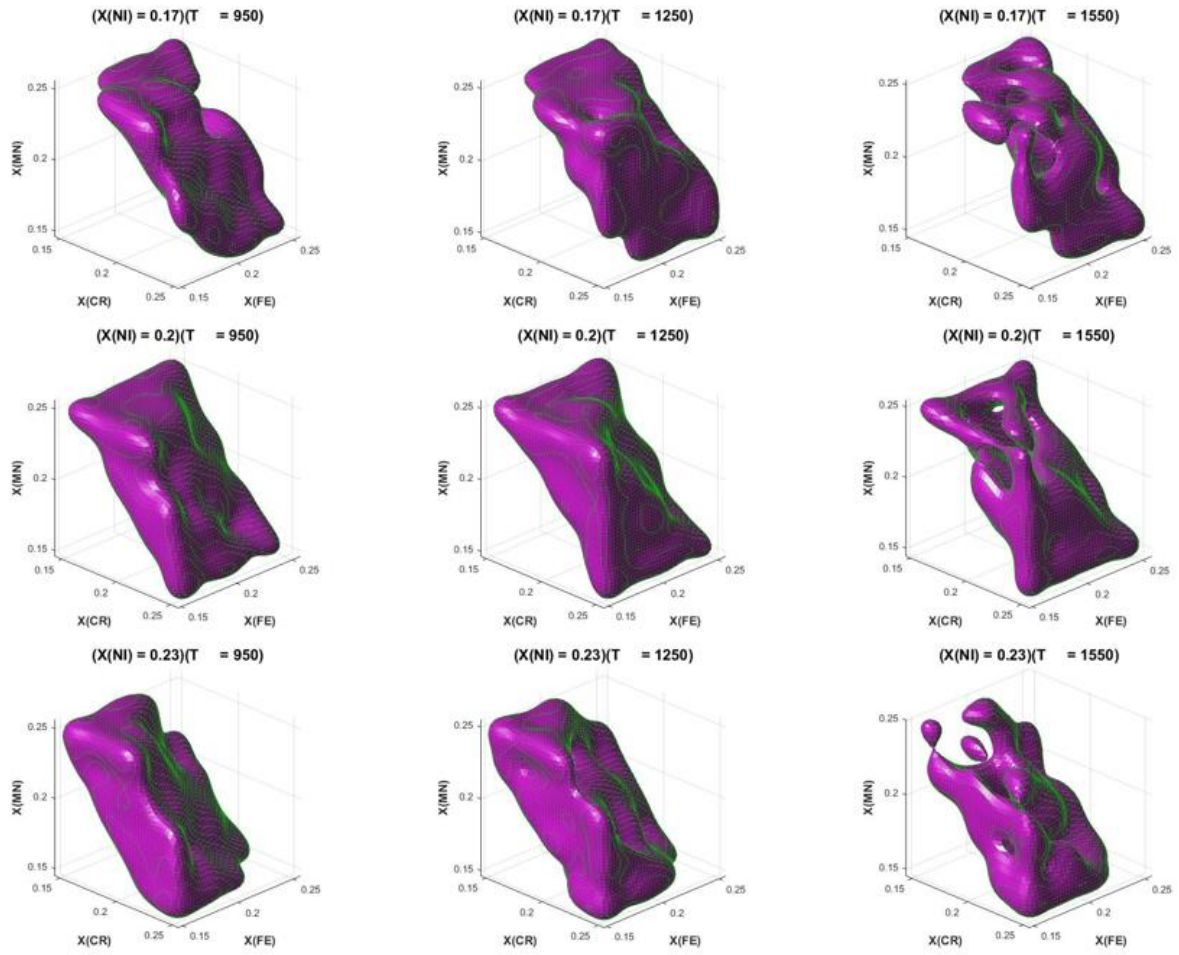

Figure 3. Evolution of L12 phase stability in CoCrFeMnNi with changes in temperature and Ni concentration

Potential precipitation hardening regions

The constraints for searching the precipitation hardening regions of AlCoCrFeNi showed a small region of BCC (within 1579 – 1642 K) and large regions of both FCC and B2 phases (within 1500 – 1654 K and 1500 – 1707 K, respectively) that could be hardened. As can be shown in Figure 4, a lower atomic concentration of Al generally results in having an FCC (red) region ready to transition to a two-phase region, while higher Al concentrations results in having

a B2 (black) region ready to transition to a two-phase region. Section D in the Appendix shows more plots at selected temperatures and Al concentrations.

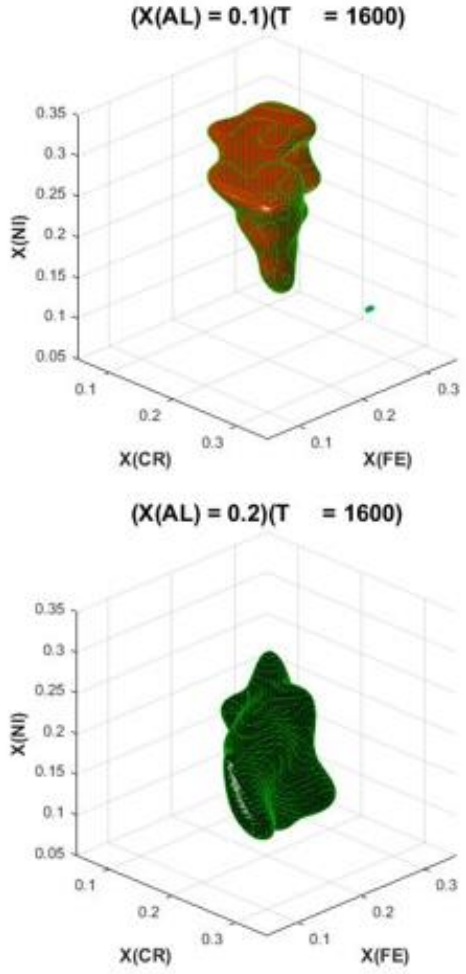

Figure 4. Change in hardenable region with change in Al concentration

CHAPTER IV

CONCLUSION

The single-phase solid solution searches with the CCSA proves that the code can be used to model the evolution of phase stability in multi-component systems such as HEAs. This can be used as a tool to discover and design new alloys to have specific phases, thereby tailoring alloys to have desired properties. The CCSA can also be used to determine alloy compositions that might be susceptible to certain processing conditions, such as precipitation hardening. Examples of three-, four-, and five-dimensional searches in the CCSA were tested against classification metrics and have been found to have relatively high precision and recall rates and relatively low misclassification rates. This proves that the combination of the CCSA and Thermo-Calc can act as a reliable framework to help accelerate HEA discovery and design. However, this is dependent on the accuracy of the Thermo-Calc database. The TCHEA1 database was found to have 70.8% agreement with experimental data. Given the complexity of HEA study, it is hard to determine whether the faults lie with Thermo-Calc in the form of thermodynamic or numerical errors, or with experimental techniques such as not allowing enough time for thermodynamic equilibrium to occur. Regardless, the discussed framework allows for experimentalists to focus on a desired composition and temperature space in HEA design without having to resort to exhaustive approaches. Future work could include collaborating with experimentalists, searching systems with more than five components, and attempting to incorporate kinetic models in the algorithm.

REFERENCES

[1] J.-W. Yeh, S.-K. Chen, S.-J. Lin, J.-Y. Gan, T.-S. Chin, T.-T. Shun, C.-H. Tsau, S.-Y. Chang, Nanostructured High-Entropy Alloys with Multiple Principal Elements: Novel Alloy Design Concepts and Outcomes, Adv. Eng. Mater. 6 (2004) 299–303. doi:10.1002/adem.200300567.

[2] M.-H. Tsai, J.-W. Yeh, High-Entropy Alloys: A Critical Review, Materials Research Letters. 2 (2014) 107–123. doi:10.1080/21663831.2014.912690.

[3] Y. Zhang, T.T. Zuo, Z. Tang, M.C. Gao, K.A. Dahmen, P.K. Liaw, Z.P. Lu, Microstructures and properties of high-entropy alloys, Progress in Materials Science. 61 (2014) 1–93. doi:10.1016/j.pmatsci.2013.10.001.

[4] D.B. Miracle, Critical Assessment 14: High entropy alloys and their development as structural materials, Materials Science and Technology. 31 (2015) 1142–1147. doi:10.1179/1743284714Y.0000000749.

[5] E. Galvan, J. Malak Richard J., S. Gibbons, R. Arroyave, Constraint Satisfaction Approach to the Design of Multi-Component, Multi-Phase Alloys, (2014) V02BT03A010. doi:10.1115/DETC2014-34707.

[6] B. Cantor, I.T.H. Chang, P. Knight, A.J.B. Vincent, Microstructural development in equiatomic multicomponent alloys, Materials Science and Engineering: A. 375–377 (2004) 213–218. doi:10.1016/j.msea.2003.10.257.

[7] I. Toda-Caraballo, P.E.J. Rivera-Díaz-del-Castillo, A criterion for the formation of high entropy alloys based on lattice distortion, Intermetallics. 71 (2016) 76–87. doi:10.1016/j.intermet.2015.12.011.

[8] H.-P. Chou, Y.-S. Chang, S.-K. Chen, J.-W. Yeh, Microstructure, thermophysical and electrical properties in AlxCoCrFeNi ($0 \leq x \leq 2$) high-entropy alloys, Materials Science and Engineering: B. 163 (2009) 184–189. doi:10.1016/j.mseb.2009.05.024.

[9] Y.-F. Kao, T.-J. Chen, S.-K. Chen, J.-W. Yeh, Microstructure and mechanical property of as-cast, -homogenized, and -deformed AlxCoCrFeNi ($0 \leq x \leq 2$) high-entropy alloys, Journal of Alloys and Compounds. 488 (2009) 57–64. doi:10.1016/j.jallcom.2009.08.090.

[10] C. Li, J.C. Li, M. Zhao, Q. Jiang, Effect of alloying elements on microstructure and properties of multiprincipal elements high-entropy alloys, Journal of Alloys and Compounds. 475 (2009) 752–757. doi:10.1016/j.jallcom.2008.07.124.

[11] T.-T. Shun, C.-H. Hung, C.-F. Lee, Formation of ordered/disordered nanoparticles in FCC high entropy alloys, Journal of Alloys and Compounds. 493 (2010) 105–109. doi:10.1016/j.jallcom.2009.12.071.

[12] Y. Zhang, X. Yang, P.K. Liaw, Alloy Design and Properties Optimization of High-Entropy Alloys, JOM. 64 (2012) 830–838. doi:10.1007/s11837-012-0366-5.

[13] Y.-J. Hsu, W.-C. Chiang, J.-K. Wu, Corrosion behavior of FeCoNiCrCux high-entropy alloys in 3.5% sodium chloride solution, Materials Chemistry and Physics. 92 (2005) 112–117. doi:10.1016/j.matchemphys.2005.01.001.

[14] C.-J. Tong, Y.-L. Chen, J.-W. Yeh, S.-J. Lin, S.-K. Chen, T.-T. Shun, C.-H. Tsau, S.-Y. Chang, Microstructure characterization of Alx, Metall and Mat Trans A. 36 (n.d.) 881–893. doi:10.1007/s11661-005-0283-0.

[15] X.F. Wang, Y. Zhang, Y. Qiao, G.L. Chen, Novel microstructure and properties of multicomponent CoCrCuFeNiTix alloys, Intermetallics. 15 (2007) 357–362. doi:10.1016/j.intermet.2006.08.005.

[16] A. Durga, K.C.H. Kumar, B.S. Murty, Phase Formation in Equiatomic High Entropy Alloys: CALPHAD Approach and Experimental Studies, Trans Indian Inst Met. 65 (2012) 375–380. doi:10.1007/s12666-012-0138-5.

[17] F. Otto, Y. Yang, H. Bei, E.P. George, Relative effects of enthalpy and entropy on the phase stability of equiatomic high-entropy alloys, Acta Materialia. 61 (2013) 2628–2638. doi:10.1016/j.actamat.2013.01.042.

[18] O.N. Senkov, G.B. Wilks, D.B. Miracle, C.P. Chuang, P.K. Liaw, Refractory high-entropy alloys, Intermetallics. 18 (2010) 1758–1765. doi:10.1016/j.intermet.2010.05.014.

[19] L. Ma, L. Wang, T. Zhang, A. Inoue, Bulk Glass Formation of Ti-Zr-Hf-Cu-M (M=Fe, Co, Ni) Alloys, Materials Transactions. 43 (2002) 277–280. doi:10.2320/matertrans.43.277.

[20] O.N. Senkov, S.V. Senkova, C. Woodward, D.B. Miracle, Low-density, refractory multi-principal element alloys of the Cr–Nb–Ti–V–Zr system: Microstructure and phase analysis, Acta Materialia. 61 (2013) 1545–1557. doi:10.1016/j.actamat.2012.11.032.

[21] X. Yang, Y. Zhang, P.K. Liaw, Microstructure and Compressive Properties of NbTiVTaAlx High Entropy Alloys, Procedia Engineering. 36 (2012) P292-298. doi:10.1016/j.proeng.2012.03.043.

[22] Y. Zhang, Y.J. Zhou, J.P. Lin, G.L. Chen, P.K. Liaw, Solid-Solution Phase Formation Rules for Multi-component Alloys, Adv. Eng. Mater. 10 (2008) 534–538. doi:10.1002/adem.200700240.

[23] C.-C. Tung, J.-W. Yeh, T. Shun, S.-K. Chen, Y.-S. Huang, H.-C. Chen, On the elemental effect of AlCoCrCuFeNi high-entropy alloy system, Materials Letters. 61 (2007) 1–5. doi:10.1016/j.matlet.2006.03.140.

[24] G.-Y. Ke, S.-K. Chen, T. Hsu, J.-W. Yeh, FCC and BCC equivalents in as-cast solid solutions of AlxCoyCrzCu0.5FevNiw high-entropy alloys, Annales de Chimie. 31 (2006) 669–683.

[25] F.J. Wang, Y. Zhang, G.L. Chen, Atomic packing efficiency and phase transition in a high entropy alloy, Journal of Alloys and Compounds. 478 (2009) 321–324. doi:10.1016/j.jallcom.2008.11.059.

[26] B.S. Li, Y.P. Wang, M.X. Ren, C. Yang, H.Z. Fu, Effects of Mn, Ti and V on the microstructure and properties of AlCrFeCoNiCu high entropy alloy, Materials Science and Engineering: A. 498 (2008) 482–486. doi:10.1016/j.msea.2008.08.025.

[27] J.M. Zhu, H.F. Zhang, H.M. Fu, A.M. Wang, H. Li, Z.Q. Hu, Microstructures and compressive properties of multicomponent AlCoCrCuFeNiMox alloys, Journal of Alloys and Compounds. 497 (2010) 52–56. doi:10.1016/j.jallcom.2010.03.074.

[28] C.W. Chang, Microstructure and Properties of as-cast 10-component Nanostructured AlCoCrCuFeMoNiTiVZr High-entropy Alloy (PhD thesis),
National Tsinghua University, Taiwan, 2004.

[29] Y.J. Zhou, Y. Zhang, F.J. Wang, G.L. Chen, Phase transformation induced by lattice distortion in multiprincipal component CoCrFeNiCuxAl1−x solid-solution alloys, Applied Physics Letters. 92 (2008) 241917. doi:10.1063/1.2938690.

[30] M.-R. Chen, S.-J. Lin, J.-W. Yeh, S.-K. Chen, Y.-S. Huang, C.-P. Tu, Microstructure and Properties of Al0.5CoCrCuFeNiTix (x=0–2.0) High-Entropy Alloys, Materials Transactions. 47 (2006) 1395–1401. doi:10.2320/matertrans.47.1395.

[31] J.-W. Yeh, S.-Y. Chang, Y.-D. Hong, S.-K. Chen, S.-J. Lin, Anomalous decrease in X-ray diffraction intensities of Cu–Ni–Al–Co–Cr–Fe–Si alloy systems with multi-principal elements, Materials Chemistry and Physics. 103 (2007) 41–46. doi:10.1016/j.matchemphys.2007.01.003.

[32] Y.J. Zhou, Y. Zhang, F.J. Wang, Y.L. Wang, G.L. Chen, Effect of Cu addition on the microstructure and mechanical properties of AlCoCrFeNiTi0.5 solid-solution alloy, Journal of Alloys and Compounds. 466 (2008) 201–204. doi:10.1016/j.jallcom.2007.11.110.

[33] J.-W. Yeh, S.-J. Lin, T.-S. Chin, J.-Y. Gan, S.-K. Chen, T.-T. Shun, C.-H. Tsau, S.-Y. Chou, Formation of simple crystal structures in Cu-Co-Ni-Cr-Al-Fe-Ti-V alloys with multiprincipal metallic elements, Metall and Mat Trans A. 35 (n.d.) 2533–2536. doi:10.1007/s11661-006-0234-4.

[34] J.W. Yeh, M.H. Chuang, S.K. Chen, Y.S. Huang, M.R. Chen, S.J. Lin, Metall. Mater. Trans. A 37 (2006) 1363e1369.

[35] Z. Hu, Y. Zhan, G. Zhang, J. She, C. Li, Effect of rare earth Y addition on the microstructure and mechanical properties of high entropy AlCoCrCuNiTi alloys, Materials & Design. 31 (2010) 1599–1602. doi:10.1016/j.matdes.2009.09.016.

[36] C.-Y. Hsu, W.-R. Wang, W.-Y. Tang, S.-K. Chen, J.-W. Yeh, Microstructure and Mechanical Properties of New AlCoxCrFeMo0.5Ni High-Entropy Alloys, Adv. Eng. Mater. 12 (2010) 44–49. doi:10.1002/adem.200900171.

[37] C.-C. Juan, C.-Y. Hsu, C.-W. Tsai, W.-R. Wang, T.-S. Sheu, J.-W. Yeh, S.-K. Chen, On microstructure and mechanical performance of AlCoCrFeMo0.5Nix high-entropy alloys, Intermetallics. 32 (2013) 401–407. doi:10.1016/j.intermet.2012.09.008.

[38] C.-Y. Hsu, T.-S. Sheu, J.-W. Yeh, S.-K. Chen, Effect of iron content on wear behavior of AlCoCrFexMo0.5Ni high-entropy alloys, Wear. 268 (2010) 653–659. doi:10.1016/j.wear.2009.10.013.

[39] C.-Y. Hsu, C.-C. Juan, W.-R. Wang, T.-S. Sheu, J.-W. Yeh, S.-K. Chen, On the superior hot hardness and softening resistance of AlCoCrxFeMo0.5Ni high-entropy alloys, Materials Science and Engineering: A. 528 (2011) 3581–3588. doi:10.1016/j.msea.2011.01.072.

[40] J.M. Zhu, H.M. Fu, H.F. Zhang, A.M. Wang, H. Li, Z.Q. Hu, Microstructures and compressive properties of multicomponent AlCoCrFeNiMox alloys, Materials Science and Engineering: A. 527 (2010) 6975–6979. doi:10.1016/j.msea.2010.07.028.

[41] S.G. Ma, Y. Zhang, Effect of Nb addition on the microstructure and properties of AlCoCrFeNi high-entropy alloy, Materials Science and Engineering: A. 532 (2012) 480–486. doi:10.1016/j.msea.2011.10.110.

[42] K. Zhang, Z. Fu, Effects of annealing treatment on phase composition and microstructure of CoCrFeNiTiAlx high-entropy alloys, Intermetallics. 22 (2012) 24–32. doi:10.1016/j.intermet.2011.10.010.

[43] F.J. Wang, Y. Zhang, Effect of Co addition on crystal structure and mechanical properties of Ti0.5CrFeNiAlCo high entropy alloy, Materials Science and Engineering: A. 496 (2008) 214–216. doi:10.1016/j.msea.2008.05.020.

[44] Y.J. Zhou, Y. Zhang, Y.L. Wang, G.L. Chen, Solid solution alloys of AlCoCrFeNiTix with excellent room-temperature mechanical properties, Applied Physics Letters. 90 (2007) 181904. doi:10.1063/1.2734517.

[45] A.K. Singh, A. Subramaniam, On the formation of disordered solid solutions in multi-component alloys, Journal of Alloys and Compounds. 587 (2014) 113–119. doi:10.1016/j.jallcom.2013.10.133.

[46] S. Guo, C. Ng, J. Lu, C.T. Liu, Effect of valence electron concentration on stability of fcc or bcc phase in high entropy alloys, Journal of Applied Physics. 109 (2011) 103505. doi:10.1063/1.3587228.

[47] H.Y. Chen, C.W. Tsai, C.C. Tung, J.W. Yeh, T.T. Shun, C.C. Yang, S.K. Chen, Effect of the substitution of Co by Mn IN Al-Cr-Cu-Fe-Co-Ni high-entropy alloys, Ann. De. Chim. Sci. Des. Mater. 31 (2006) 685-698. doi:10.3166/acsm.31.685-698.

[48] M. Chen, Y. Liu, Y.X. Li, X. Chen, Microstructure and mechanical properties of $AlTiFeNiCuCr_x$ high-entropy alloy with multi-principal elements**,** Acta Metall. Sin. 43 (2007) 1020-1024.

[49] K.-C. Hsieh, C.-F. Yu, W.-T. Hsieh, W.-R. Chiang, J.S. Ku, J.-H. Lai, C.-P. Tu, C.C. Yang, The microstructure and phase equilibrium of new high performance high-entropy alloys, Journal of Alloys and Compounds. 483 (2009) 209–212. doi:10.1016/j.jallcom.2008.08.118.

[50] J.Y. Yang, Y.J. Zhou, Y. Zang, Chin. Mater. Sci. Technol. Equip. 5 (2007) 61-63.

[51] Y.J. Zhou, Y. Zhang, Y.L. Wang, G.L. Chen, Microstructure and compressive properties of multicomponent Alx(TiVCrMnFeCoNiCu)100−x high-entropy alloys, Materials Science and Engineering: A. 454–455 (2007) 260–265. doi:10.1016/j.msea.2006.11.049.

[52] T.-T. Shun, L.-Y. Chang, M.-H. Shiu, Microstructure and mechanical properties of multiprincipal component CoCrFeNiMox alloys, Materials Characterization. 70 (2012) 63–67. doi:10.1016/j.matchar.2012.05.005.

[53] Y.L. Chou, J.W. Yeh, H.C. Shih, The effect of molybdenum on the corrosion behaviour of the high-entropy alloys Co1.5CrFeNi1.5Ti0.5Mox in aqueous environments, Corrosion Science. 52 (2010) 2571–2581. doi:10.1016/j.corsci.2010.04.004.

[54] J.D. Plummer, A.J. Cunliffe, A.I. Figueroa, et al., Glassformation in a high entropy alloy, in: Presentation at the 8th international Conference on Bulk Metallic Glasses. Hong Kong, 2011.

[55] T.-T. Shun, L.-Y. Chang, M.-H. Shiu, Microstructures and mechanical properties of multiprincipal component CoCrFeNiTix alloys, Materials Science and Engineering: A. 556 (2012) 170–174. doi:10.1016/j.msea.2012.06.075.

[56] B. Ren, Z.X. Liu, D.M. Li, L. Shi, B. Cai, M.X. Wang, Effect of elemental interaction on microstructure of CuCrFeNiMn high entropy alloy system, Journal of Alloys and Compounds. 493 (2010) 148–153. doi:10.1016/j.jallcom.2009.12.183.

[57] A. K. Singh, A. Subramaniam, Thermodynamic Rationalization of the Microstructures of CrFeNi & CuCrFeNi Alloys, Advanced Materials Research. 585 (2012) 3-7. doi:10.4028/www.scientific.net/AMR.585.3

[58] O.N. Senkov, J.M. Scott, S.V. Senkova, D.B. Miracle, C.F. Woodward, Microstructure and room temperature properties of a high-entropy TaNbHfZrTi alloy, Journal of Alloys and Compounds. 509 (2011) 6043–6048. doi:10.1016/j.jallcom.2011.02.171.

[59] E. Galvan, R.J. Malak, S. Gibbons, R. Arroyave, A Constraint Satisfaction Algorithm for the Generalized Inverse Phase Stability Problem, Journal of Mechanical Design. 139 (2016) 11401-11401–11. doi:10.1115/1.4034581.

[60] Y.-F. Kao, T.-J. Chen, S.-K. Chen, J.-W. Yeh, Microstructure and mechanical property of as-cast, -homogenized, and -deformed AlxCoCrFeNi ($0 \leq x \leq 2$) high-entropy alloys, Journal of Alloys and Compounds. 488 (2009) 57–64. doi:10.1016/j.jallcom.2009.08.090.

APPENDIX

A. Thermo-Calc graphs

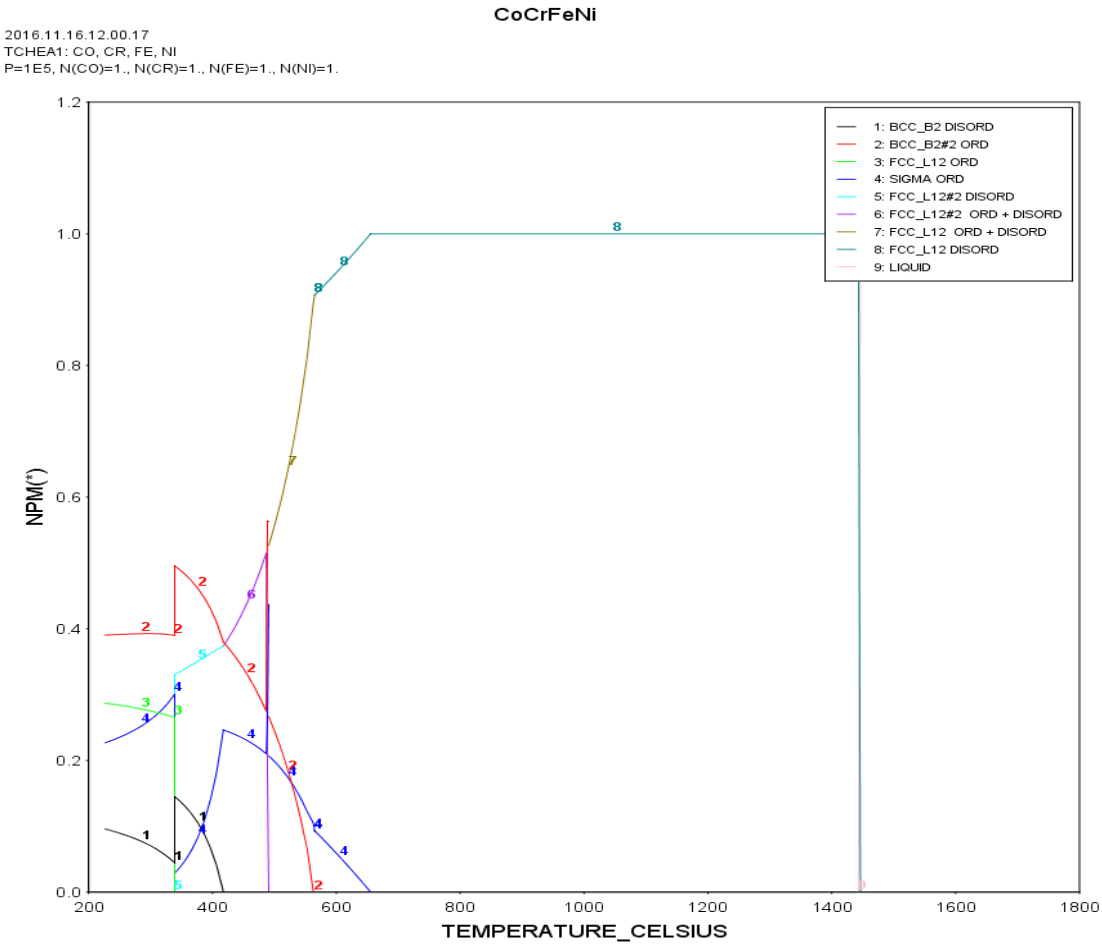

Figure A1. Phase stability graph output from Thermo-Calc software

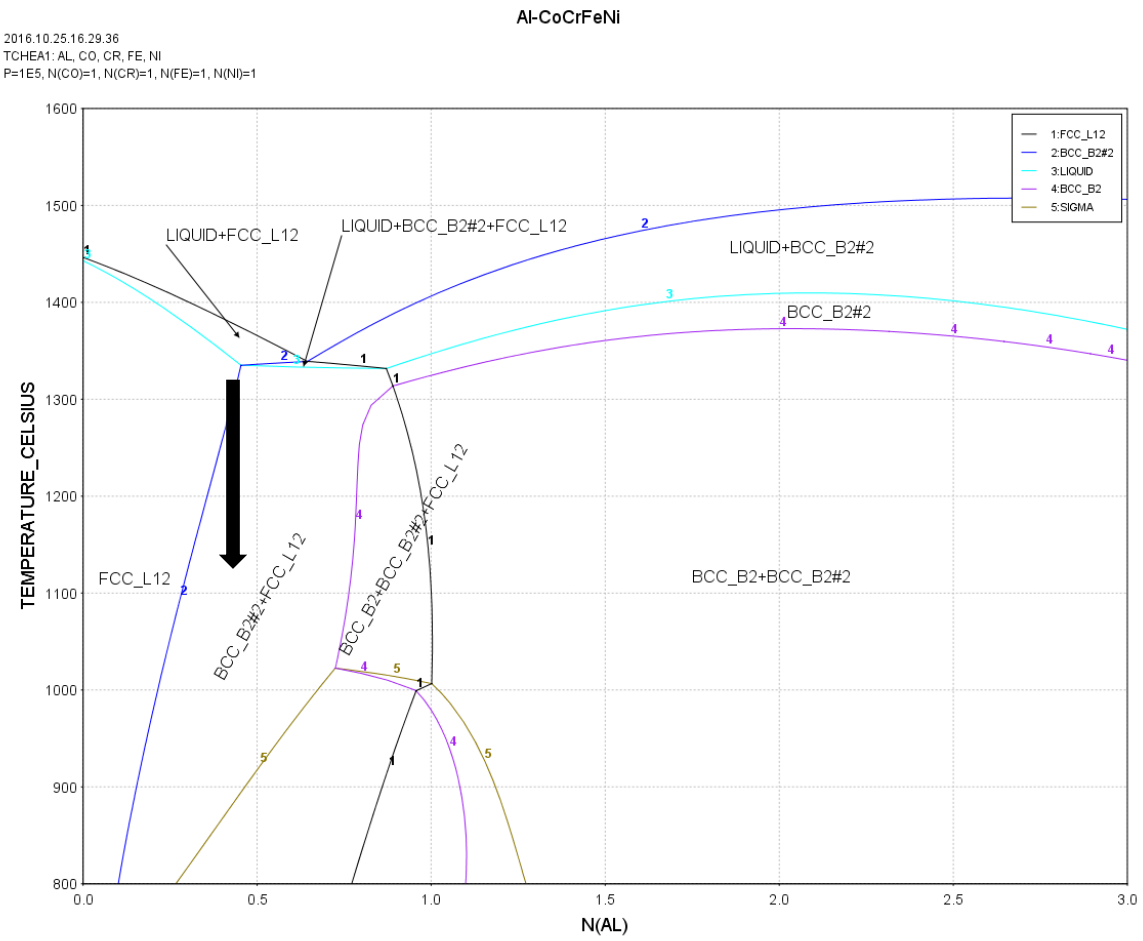

Figure A2. AlCoCrFeNi isopleth showing a two-phase region under a single-phase solid solution region

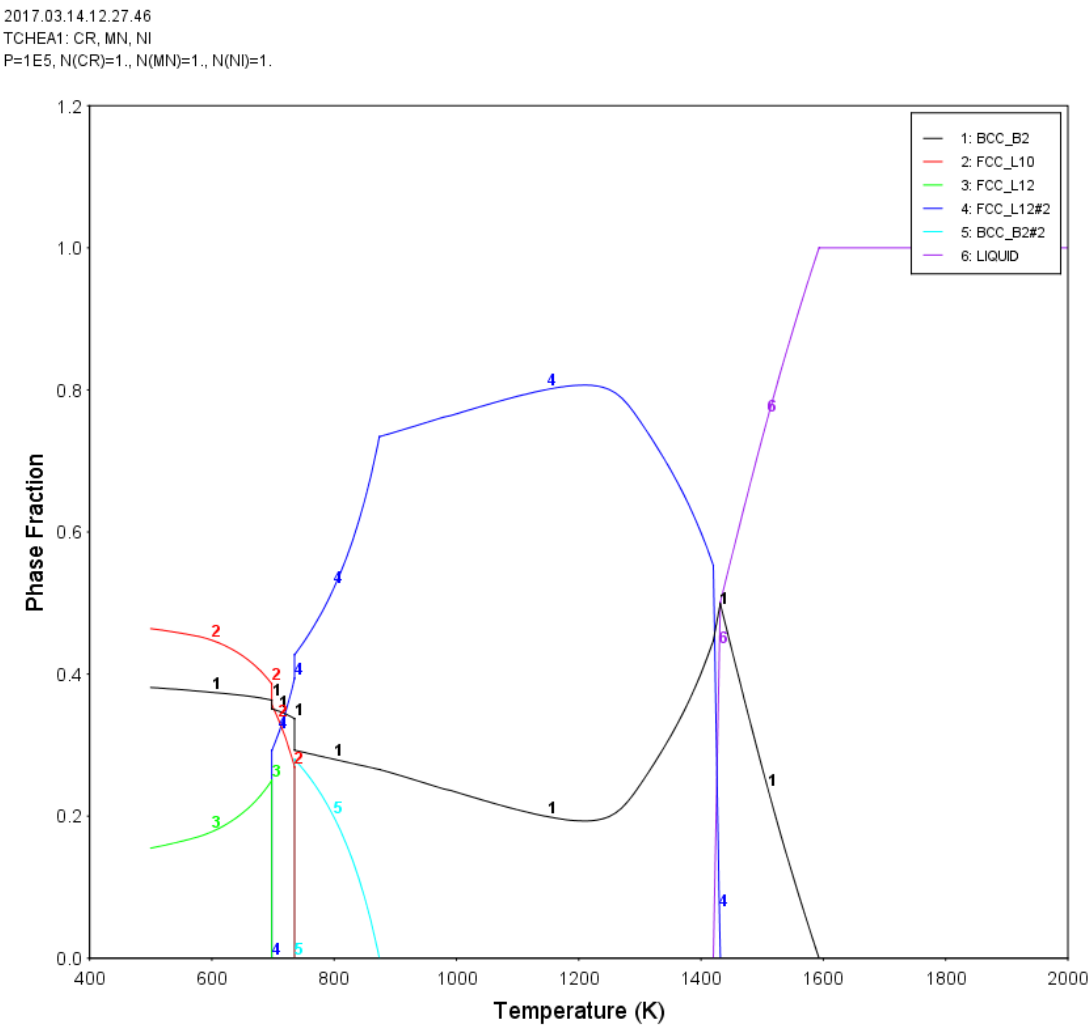

Figure A3. Phase fraction graph of CrMnNi at an equiatomic concentration

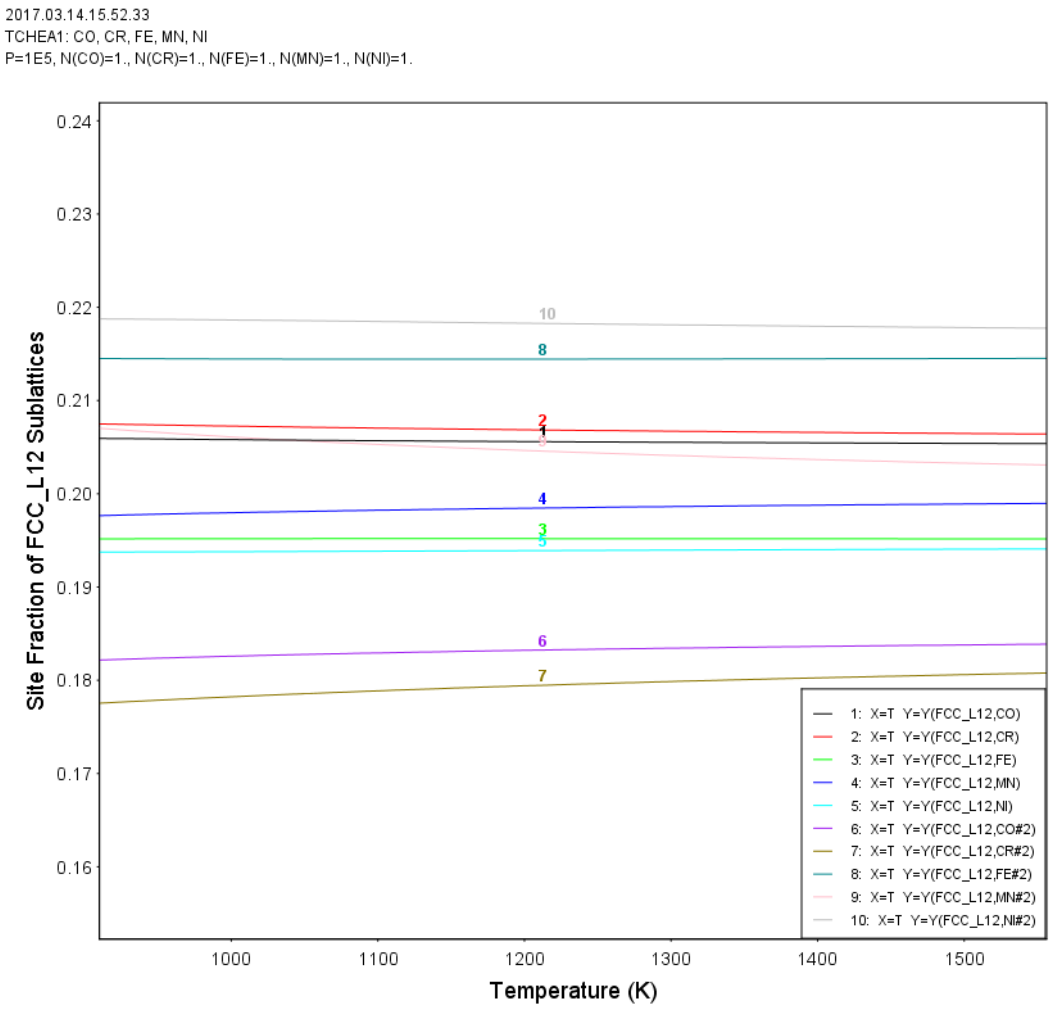

Figure A4. Site fractions of FCC_L12 sublattices in CoCrFeMnNi between 1000-1500 K

Legend for Sections B, C, and D

B. Ternary visualizations

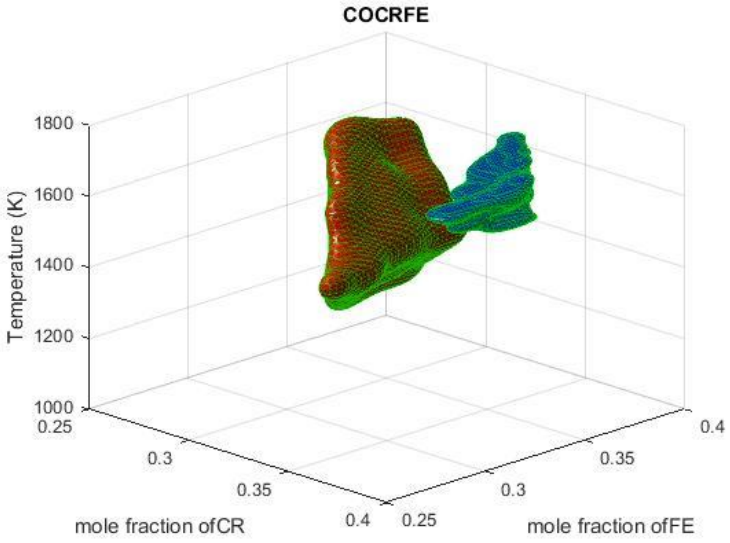

Figure B1. Single-phase region visualization for CoCrFe

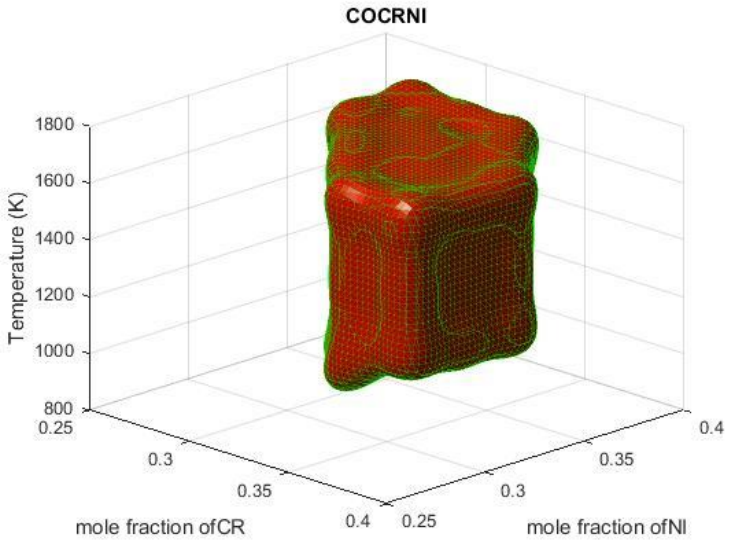

Figure B2. Single-phase region visualization for CoCrNi

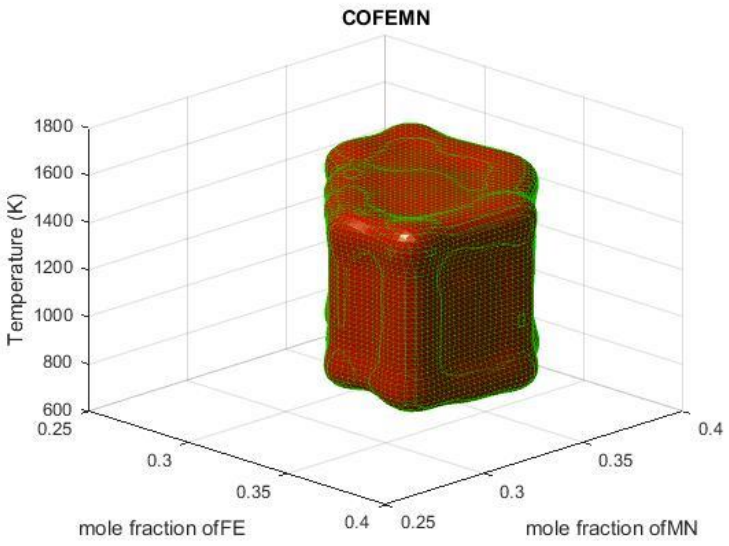

Figure B3. Single-phase region visualization for CoFeMn

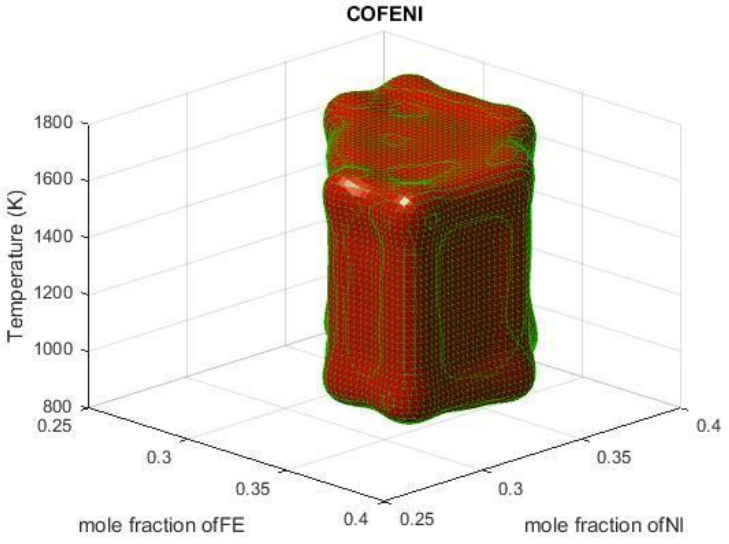

Figure B4. Single-phase region visualization for CoFeNi

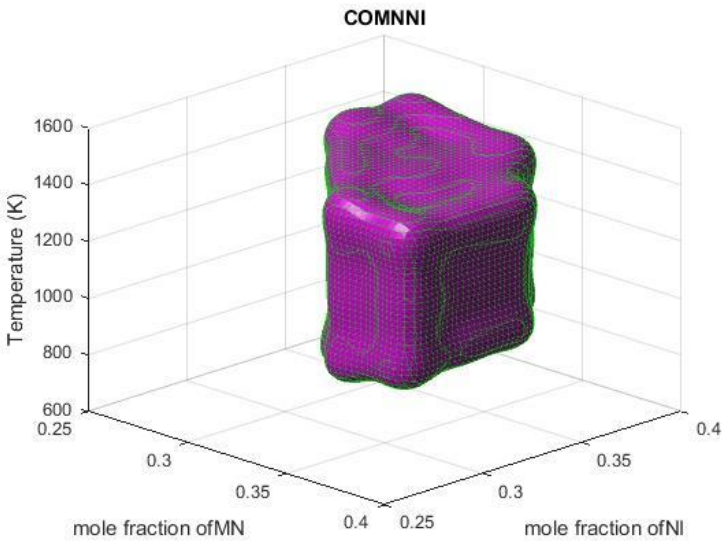

Figure B5. Single-phase region visualization for CoMnNi

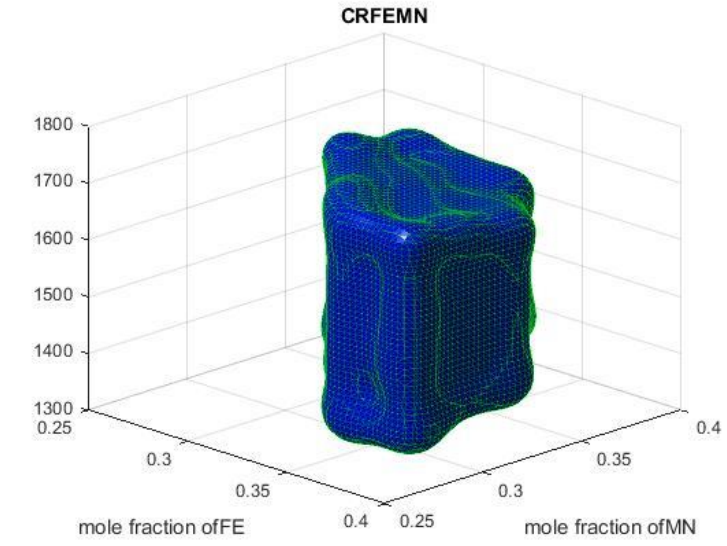

Figure B6. Single-phase region visualization for CrFeMn

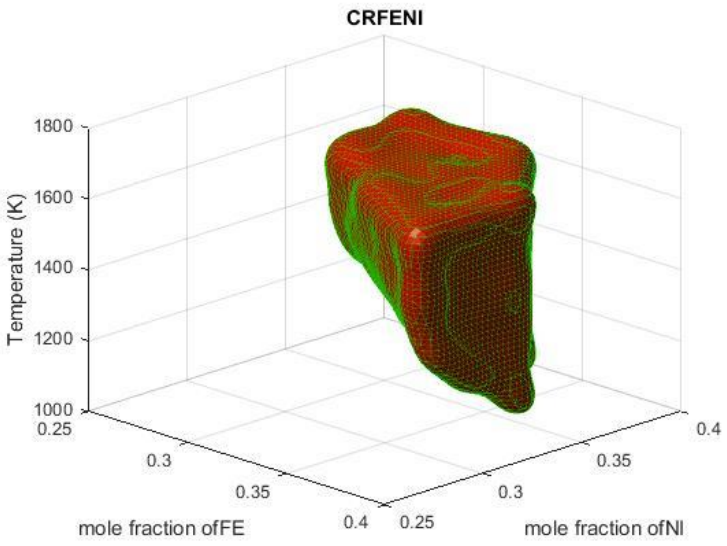

Figure B7. Single-phase region visualization for CrFeNi

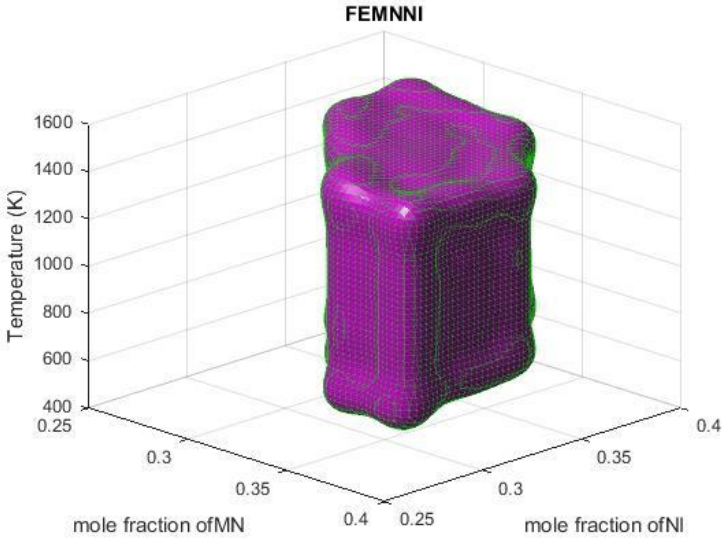

Figure B8. Single-phase region visualization for FeMnNi

C. Quaternary visualizations

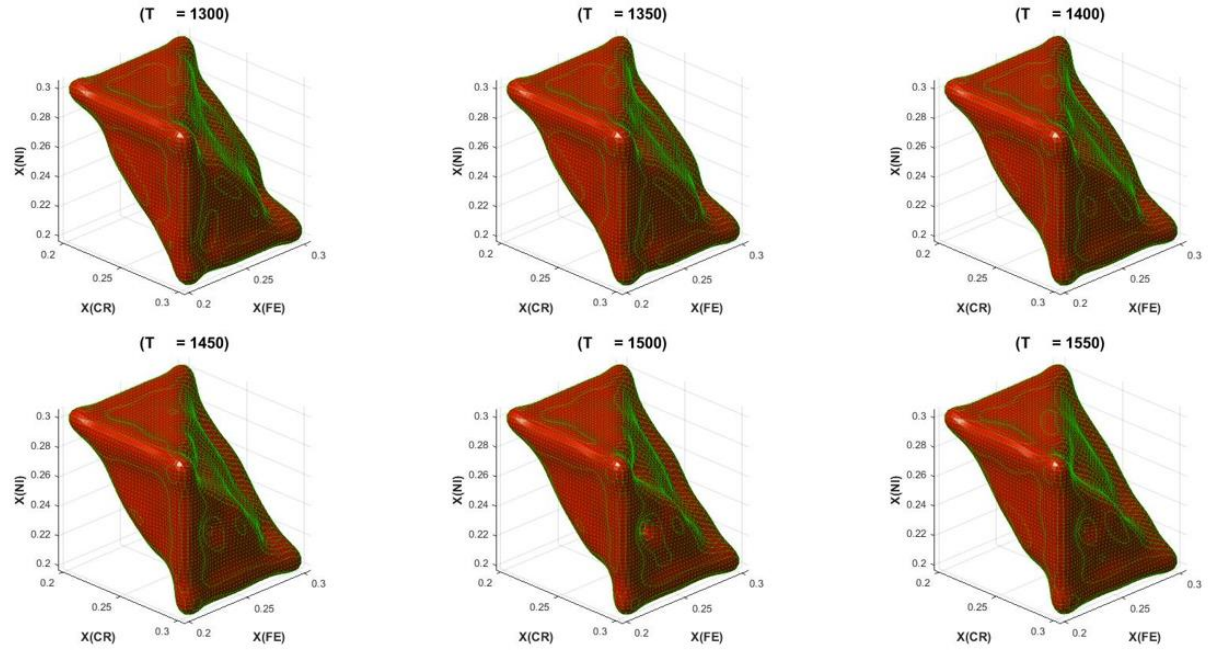

Figure C1. Single-phase region visualizations for selected temperatures in CoCrFeNi

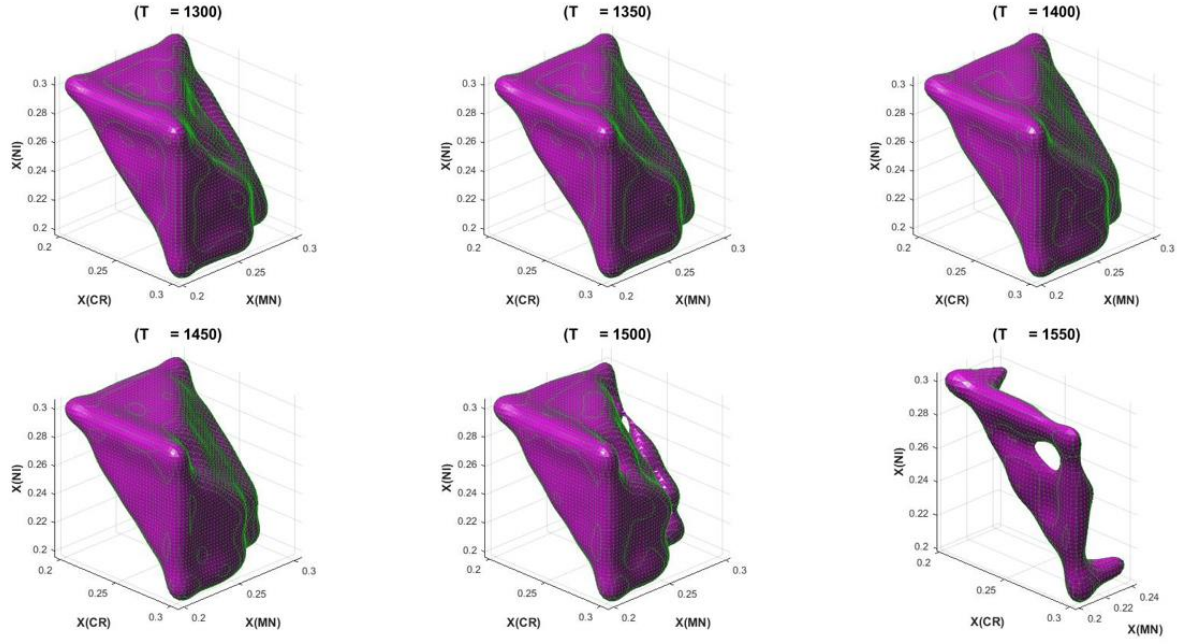

Figure C2. Single-phase region visualizations for selected temperatures in CoCrMnNi

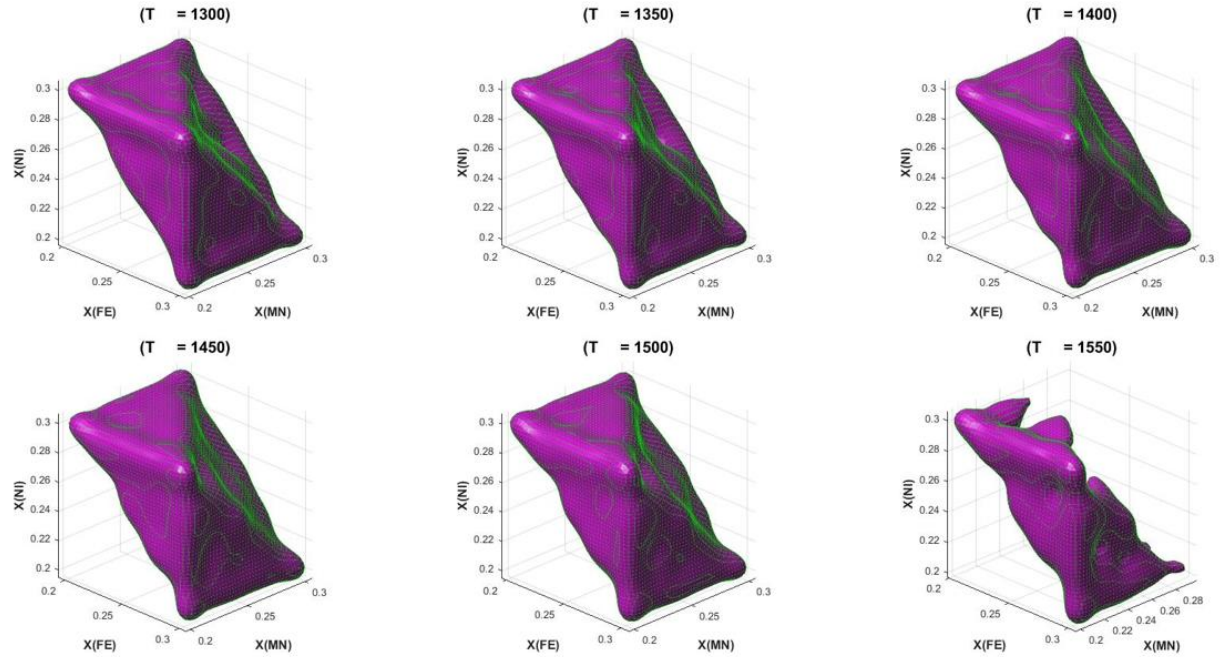

Figure C3. Single-phase region visualizations for selected temperatures in CoFeMnNi

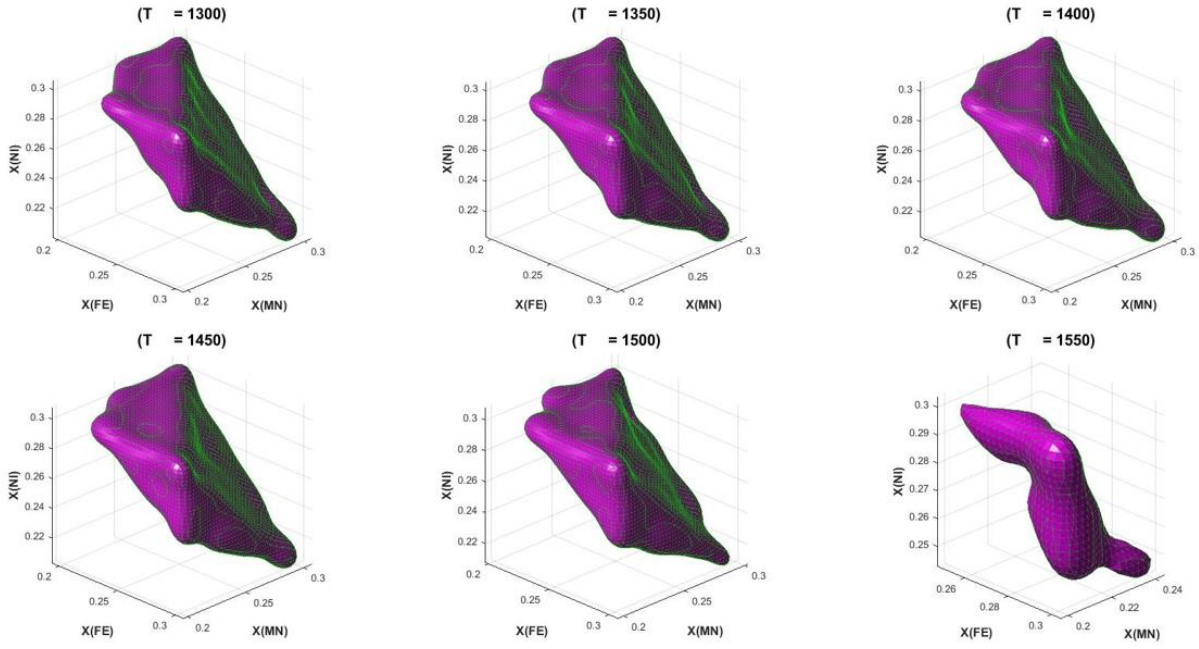

Figure C4. Single-phase region visualizations for selected temperatures in CrFeMnNi

D. Precipitation hardening (AlCoCrFeNi)

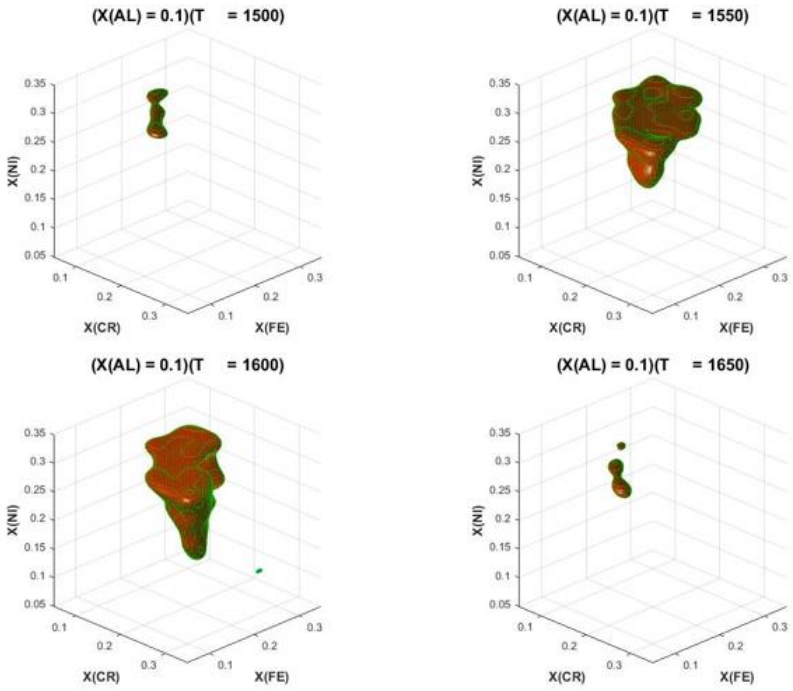

Figure D1. Regions of precipitation hardenability with 10% atomic concentration of Al

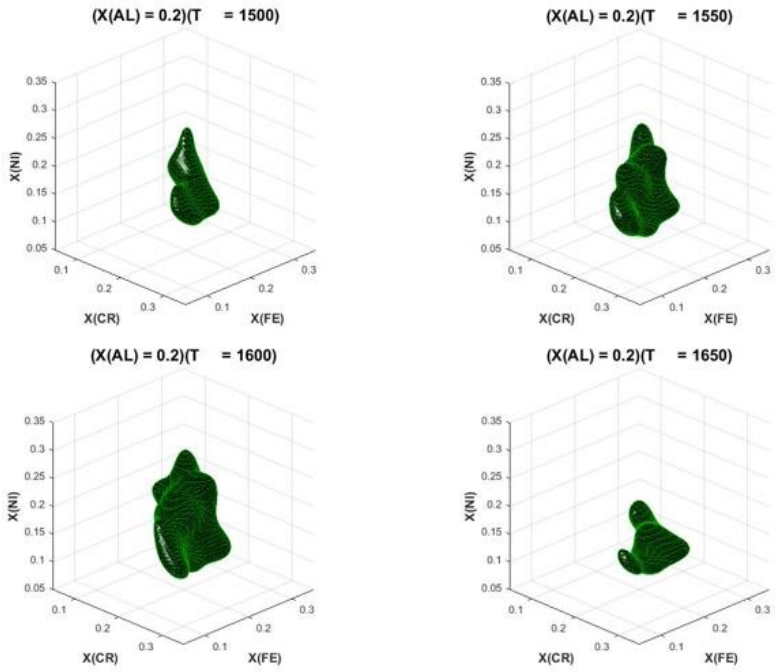

Figure D2. Regions of precipitation hardenability with 20% atomic concentration of Al

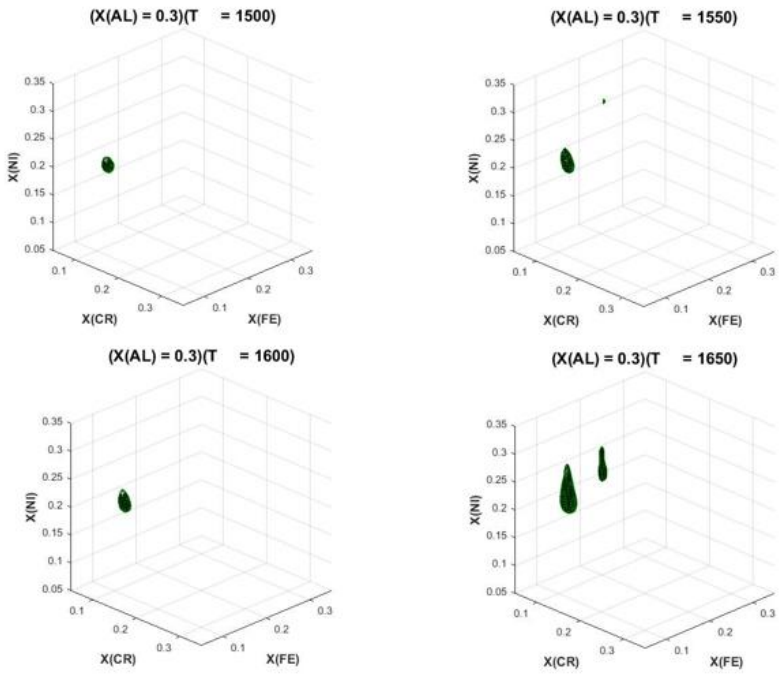

Figure D3. Regions of precipitation hardenability with 30% atomic concentration of Al